Ratiometric luminescence 2D *in vivo* imaging and monitoring of mouse skin oxygenation

2013 Methods Appl. Fluoresc. 1 045002

(http://iopscience.iop.org/2050-6120/1/4/045002)

Methods Appl. Fluoresc. **1** (2013) 045002 (9pp) doi:10.1088/2050-6120/1/4/045002

Ratiometric luminescence 2D *in vivo* imaging and monitoring of mouse skin oxygenation

Julian Hofmann[1], Robert J Meier[2], Alexander Mahnke[1], Valentin Schatz[1], Florian Brackmann[3], Regina Trollmann[3], Christian Bogdan[1], Gregor Liebsch[4], Xu-dong Wang[2], Otto S Wolfbeis[2] and Jonathan Jantsch[1]

[1] Mikrobiologisches Institut-Klinische Mikrobiologie, Immunologie und Hygiene, Universitätsklinikum Erlangen, Friedrich-Alexander Universität Erlangen-Nürnberg, Wasserturmstraße 3-5, D-91054 Erlangen, Germany
[2] Institut für Analytische Chemie, Chemo- und Biosensorik, Universität Regensburg, Universitätsstraße 31, D-93053 Regensburg, Germany
[3] Kinder- und Jugendklinik, Abteilung Neuropädiatrie, Universitätsklinikum Erlangen, Friedrich-Alexander Universität Erlangen-Nürnberg, Loschgestraße 15, D-91054 Erlangen, Germany
[4] Presens GmbH, Josef-Engert-Straße 11, D-93053 Regensburg, Germany

E-mail: Jonathan.Jantsch@uk-erlangen.de

Received 14 May 2013, in final form 5 July 2013
Published 12 August 2013
Online at stacks.iop.org/MAF/1/045002

Abstract
Tissue oxygenation plays a critical role in the pathogenesis of various diseases, but non-invasive, robust and user-friendly methods for its measurement *in vivo* still need to be established. Here, we are presenting an *in vivo* oxygen-detection system that uses ratiometric luminescence imaging (RLI) as a readout scheme to determine the skin oxygen tension of mouse hind footpads via side-by-side comparison with more established techniques including luminescence-lifetime imaging using planar sensor films and the polarographic electrode as the gold standard. We also demonstrate that this technology allows the detection of changes in mouse skin tissue oxygenation induced by subjecting mice to systemic hypoxia. The data demonstrate oxygen imaging based on RLI to be a most useful tool for reliably and easily analyzing and monitoring skin tissue oxygenation *in vivo*. This technology will advance our understanding of local regulation of skin tissue oxygenation in various disease conditions.

Acronyms

CCD	charged-coupled device
EPR	electron paramagnetic resonance imaging
EF5	2-2-nitro-1H-imidazol-1yl-*N*-(2,2,3,3,3)-pentafluoropropyl acetamide
LED	light-emitting diode
LLI	luminescence-lifetime imaging
RLI	ratiometric luminescence imaging
Hct	hematocrit
PET	positron emission tomography
$p_{ti}O_2$	skin oxygen tissue tension
$p_{tc}O_2$	transcutaneous skin oxygen tension
RGB	red, green, blue

1. Introduction

Cancer and ischemia are well-established pathological conditions leading to severe tissue hypoxia [1–3]. Infections and inflammation in living organisms are thought to be frequently associated with low oxygen tensions in the afflicted tissues [4]. Given the fact that hypoxia is a key modulator of cell-biological and immunological processes, there is

an increasing interest in understanding the role of tissue oxygenation in various diseases [5].

Various methods have been established to determine and visualize tissue oxygenation. For example, researchers have used (a) 2-nitroimidazole derivatives that allow staining of hypoxic tissues, (b) oxygen-sensitive radiolabeled or paramagnetic tracers, (c) the property of hemoglobin to change its spectroscopic or magnetic properties with its degree of oxygenation, (d) polarographic oxygen sensors and (e) phosphorescent dyes that quench luminescence in an oxygen-dependent manner.

Positron emission tomography (PET) and electron paramagnetic resonance imaging (EPR) allow for the detection of hypoxic areas after injection of either radiolabeled or paramagnetic oxygen tracers. However, these methods have a low spatial resolution and are not easily implemented [6, 7].

Visualization of hypoxic areas with microscopical resolution in histological specimens, can be achieved by using 2-nitroimidazole derivatives. These compounds (e.g., pimonidazol, EF5) need to be injected into mice prior to obtaining the tissue specimens, accumulate in areas with an oxygen tension below ∼10 Torr and form adducts that can be detected by immunohistochemical methods. While this technique gives exact information on severely hypoxic regions, it neither provides quantitative data on tissue oxygenation nor allows continuous monitoring of oxygen supply over time [8–12].

Accepted methods to indirectly quantify tissue oxygenation rely on the property of hemoglobin to change its spectroscopic or magnetic properties with its degree of oxygenation. This chemical behavior offers the estimation of tissue oxygenation by calculating the ratio of oxygenated to non-oxygenated hemoglobin. However, the methods are known to be imprecise and again do not provide exact values for tissue oxygenation (reviewed in [13, 14]).

Thus, polarographic oxygen sensors are still considered to be the 'gold standard' for sensing oxygen. Multiwire electrodes can be placed on the surface or needle-electrodes are pushed into the tissue [15, 16]. Such electrodes consist of a noble metal, on which oxygen is reduced due to a negative polarizing voltage and thus generates a current to flow. This results in a potential difference between the reference electrode (anode) and the measuring electrode (cathode) that is proportional to the amount of oxygen molecules being reduced on the cathode (reviewed in: [13]). However, electrodes consume oxygen, precise positioning is tedious, and the electrode only allows for single-spot measurements.

An alternative approach for sensing and imaging of oxygen is based on luminescence quenching of dyes [13, 14, 17–19]. Oxygen concentration can be determined by measuring luminescence intensities [20], or by other techniques, such as luminescence-lifetime imaging (LLI) [21–23] or the signals at two wavelengths (ratiometry) [24–27]. In order to determine tissue oxygenation these dyes may be used (a) bound to albumin ([14] and literature cited therein), (b) after modification with poly(ethylene glycol) residues [28] or (c) immobilized into sensor foils that contain an oxygen-permeable polymer matrix layer ([13, 29] and references cited therein). The former two methods require injection of the dye, while sensor foil-based imaging is easy to perform since it only requires the deposition of a non-invasive sensor on skin or tissue and epi-illumination of the sensor with appropriate devices that allow either detection of luminescence lifetime or intensity.

In the present study, we evaluated ratiometric luminescence imaging (RLI)-based oxygen imaging using sensor foils via a side-by-side comparison of skin oxygen tensions of hind footpads of non-anesthetized mice using different oxygen measurement techniques, including 2D-LLI imaging using planar sensor films and one-spot determination via the polarographic electrode. Finally, we demonstrate that this technique allows the detection of changes in mouse skin tissue oxygenation induced by subjecting mice to systemic hypoxia.

2. Materials and methods

2.1. Preparation of mice for oxygen imaging

All mice were bred and kept following the animal welfare protocol approved by the government of Middle Franconia (registration no. 54-2592.1-31/10 and 54-2592.1-7/12).

Under ambient air conditions and at a room temperature of 23–24 °C female C57BL/6 mice (Charles River Breeding Laboratories, Sulzfeld, Germany) were restrained and the hind leg was placed on a heating foil (thermo Technologies, purchased via Conrad Elektronik, Nürnberg, Germany) for approximately 5 min in order to set the temperature at the measuring site to 40 °C in order to increase the oxygen permeability of the epidermis and in order to maintain a constant blood flow in the dermal and epidermal vessels [30–34]. Temperature was monitored with a infrared thermometer (IR 900-30S, Voltcraft purchased via Conrad Elektronik; absolute temperature accuracy as specified by the manufacturer: ±1.5%/±1 °C).

2.2. Oxygen-sensing using the polarographic electrode technique

According to the manufacturer's instructions, the sharpened Clark-type microelectrodes (Ox-100, Unisense, Aarhaus, Denmark) were prepolarized for at least two hours and were two-point calibrated in either deoxygenated (using $Na_2S_2O_5$) or air-saturated 37 °C water prior to use. The tissue oxygenation of the mice feet was determined using the Clark-type microelectrodes. For that purpose, sharpened microelectrodes (100 μm in diameter) were advanced into the heated skin of the footpad. For standardized measurements, the oxygen microelectrode was mounted on a micromanipulator and inserted vertically from the surface to a point where a stable $p_{ti}O_2$ signal was obtained (approx. 100–400 μm depth). The measurements were recorded and data were evaluated using the provided Sensor Trace PRO 3.1.3 software (Unisense).

2.3. Oxygen-sensing using oxygen-sensitive sensor foils along with ratiometric imaging or luminescence lifetime as readout

Measurements using ratiometric luminescence imaging (RLI)- or luminescence-lifetime imaging (LLI)-based optical readouts were performed. Each mouse foot was fixed on a self-adhesive heating foil. The measurements took place after 5 min of equilibration time in order to set the temperature at the measuring site to 40 °C. A drop of water was deposited on the foot prior to covering it with a luminescent oxygen-sensor foil. The sensor foil can be cut into small pieces in almost any desired shape. Thereby, the foil was in close contact with the skin. We ensured that there were no air bubbles between sensor and foot that would result in erroneous measurements. The sensor was additionally fixed on the mouse foot using a transparent adhesive tape. No excessive pressure was applied to the foot. Sensor foils for RLI and LLI contain both an oxygen-dependent probe that generates an oxygen-dependent signal by collisional quenching of luminescence. The oxygen indicator molecules in their excited triplet state collided with triplet oxygen in its relaxed state. Therefore, the energy was transferred from the dye to the oxygen molecules resulting in deactivation of the indicators excited state. The electronically excited oxygen molecule then relaxed without the generation of visible light. Thus, in contrast to polarographic electrode technique no oxygen was consumed.

2.3.1. Ratiometric luminescence imaging (RLI) of oxygen. The RLI-sensor consisted of a transparent oxygen-sensitive foil (prototype oxygen-sensor set SF-RPSu4-NAU-L4/W4-OIW, PreSens, Regensburg, Germany) and a portable RLI-device (USB (universal serial bus) microscope 'VisiSens' A1 prototype; PreSens GmbH). The VisiSens AnalytiCal1 software provided control of the camera settings and was used to analyze the data. The sensors used in this study (SF-RPSu4-NAU-L4/W4-OIW) are part of the commercially available imaging system VisiSens and are optimized for working together with the VisiSens® hardware and software in terms of spectral response, signal amplitudes, dynamics and other material properties which are essential for robust calibration and processing.

The sensor foil consisted of a red luminescent oxygen-dependent probe and a green luminescent reference dye both immobilized in a highly oxygen-permeable polymer matrix to form a sensor layer (6–8 μm thickness) which was fixed on a transparent and oxygen-blocking polyester support ($\sim$20 μm thickness). This ensured that the sensor detects only oxygen on the side of the sensor layer that was faced towards the mouse tissue. The platinum(II) complex of tetrakis(pentafluorophenyl)porphyrin (PtTFPP) served as a probe for oxygen. It can be photoexcited at 400–420 nm to give a red emission band peaking at 650 nm. The dye N-(5-carboxypentyl)-4-piperidino-1,8-naphthalimide with its fairly narrow green fluorescence band peaking at 510 nm served as an unquenchable reference dye. Other aminonapthalimides may also be used. Both the probe and the reference dye were incorporated into a commercially available polyurethane hydrogel as described by Wang *et al* [24]. The oxygen-sensitive probe and reference dye were excited by epi-illuminating the sensor foil with blue LEDs (incorporated into the RLI-device). A color RGB-chip on the reverse side of the RLI-device detected the emitted red and green signals from the sensor foil. It is possible to use the sensors in a repetitive manner. Sensors can be cleaned with 70% ethanol or sterilized by gamma-irradiation. The sensor should be recalibrated if excitation time exceeds 72 h.

The virtual resolution of the RLI-system is about 12 μm (given a working distance of 2 cm and an imaging area 15 mm $\times$ 12 mm). Due to lateral diffusion of oxygen according to Fick's law and assuming Gaussian distribution of pixel noise, the typical true spatial resolution was 60 μm $\times$ 60 μm. If smaller areas or a profile of phase transition gradients are analyzed averaging of several images will reduce noise. However, this requires that the sample is in steady state and that the analyzed sample does not display any changes in oxygenation within the time period of image recording.

The RLI-sensor was pre-calibrated with gases of different (%) O_2-levels generated by a gas-mixing device. Prior to use, the RLI-sensor foils were two-point calibrated using $Na_2S_2O_5$ and air-saturated distilled water. Signals were generated and detected in a darkened environment by a portable RLI-device (VisiSens® A1 prototype) that was mounted on a tripod and connected via universal serial bus to a computer unit.

2.3.2. Luminescence-lifetime imaging (LLI) of oxygen. LLI was performed by epi-illumination using a system composed of a time-gated 12-bit CCD camera (TGI, Photonic Research Systems) equipped with a pulsed 460 nm LED array (Luxeon V Star LXHL-LB5C, 5W, Philips Lumileds Lighting Company, San Jose, CA, USA) as excitation light source and a 800/60 nm bandpass emission filter (Omega Optical, Brattleboro, VT, USA) in front of the camera lens [35]. The luminescent dye palladium(II)-meso-tetraphenyl-tetrabenzoporphyrin (Sigma Aldrich, Talkirchen, Germany) was used as oxygen probe, which was incorporated in a 6 μm thick oxygen-permeable polystyrene sensor layer that was immobilized on a transparent, but oxygen-blocking Saran® food barrier wrap (acts as sensor support). Together these two layers form the oxygen-sensitive sensor foils. This setup ensured that the sensor detects only oxygen on the side of the sensor layer. The sensor layer was faced towards the mouse tissue. Oxygen-dependent luminescent lifetime was measured via the LLI method. The luminescence decay time τ for self-referenced measurements was calculated by the following equation: $\tau = (t_2 - t_1)/\ln(A_{t_1}/A_{t_2})$. The luminescence intensities (A) were obtained after $t_1 = 1$ μs and $t_2 = 31$ μs. Gate width was set to 30 μs each. For ease of use, another, but simpler calculation of oxygen-dependent signals was accomplished: after pre-calibration, dividing the ratio A_{t_1}/A_{t_2} provides virtually linear relationship ($R^2 = 0.999\,34$) towards oxygenation in the relevant range of this measurement and was used for *in vivo* experiments. The measurements were performed in a darkened environment. Data were analyzed with the provided software (Image X TG1 v. 4.0, Salford, UK). The ROI of the measurement was defined

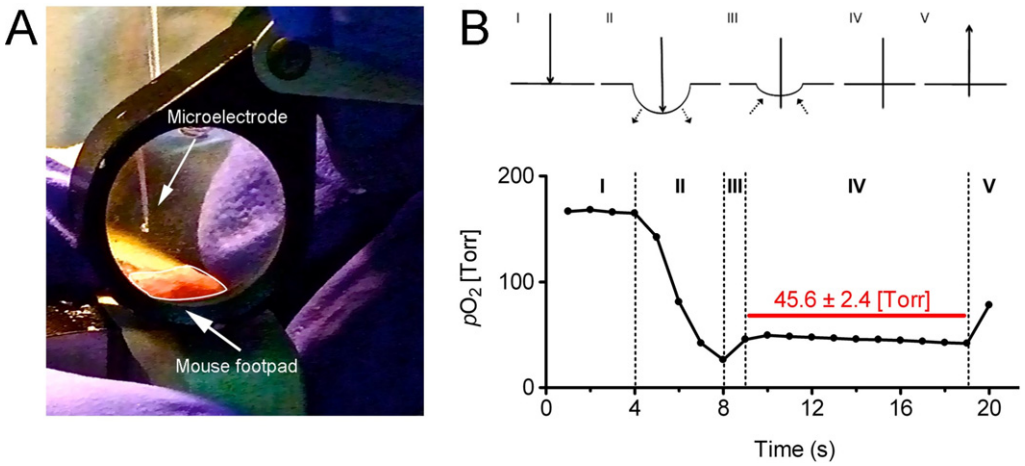

Figure 1. Determination of skin oxygen tension using a Clark-type polarographic microelectrode. (A) Photograph through a magnifying lens (6×) of the setup including the sharpened microelectrode (100 μm diameter) and the mouse footpad (time frame I). (B) Scheme of the steps in continuously recording of oxygen tension in the skin using the Clark-type microelectrode (in Torr). Time frame (I): the microelectrode was brought in contact with the skin. Time frame (II): pressure exerted by the tip of the microelectrode before penetration of the skin. Time frame (III): penetration of the skin. Time frame (IV): cessation of microelectrode advancement and recording of skin oxygen tension (here: approx. 10 s, mean: 45.6 ± 2.4 Torr). The oxygen content during time frame IV decreases due to consumption of oxygen by the electrode. Time frame (V): removal of the electrode.

as an area of 40 times 40 pixels in the center of the adopted sensor. LLI-sensor foils were pre-calibrated with different (%) O_2-levels generated by a gas-mixing device.

2.4. Experiments with animals kept under conditions of chronic hypoxia

For studies under conditions of chronic hypoxia, mice were exposed to 9% O_2 for 10 days in an animal hypoxia chamber (Biospherix Ltd, Lacona, NY, USA). Normoxic control mice were kept under ambient air conditions. RLI of oxygen was performed under normoxic or hypoxic conditions.

2.5. Hematocrit measurements

Blood was collected in EDTA tubes (GK 150, KABE, Nümbrecht, Germany) and analyzed for hematocrit based on red blood cell count and volume using an automated hematology analyzer (Sysmex XS 800i, Sysmex, Norderstedt, Germany).

2.6. Statistical analysis

Statistical significance was calculated with the Prism v4.0 GraphPad software. Student's *t* test or analysis of variance (ANOVA) was used to analyze data. *P* values less than 0.05 were considered significant.

3. Results and discussion

3.1. Determination of skin oxygenation using a Clark-type microelectrode

Clark-type microelectrodes were used to determine mouse skin oxygen tissue tension of hind footpads ($p_{ti}O_2$). A sharpened Clark-type microelectrode (100 μm in diameter) was advanced onto (figures 1(A) and (B), time frame I–II) and through the skin using a micromanipulator. The pressure exerted by the tip of the Clark-type electrode caused local ischemia of the skin tissue just before the microelectrode penetrated the skin (figure 1(B), time frame II). After penetration of the skin, the local pressure and hence the pressure-induced local ischemia were immediately relieved. This resulted in an increase of the recorded oxygen tension (figure 1(B), time frame III). The microelectrode was not further advanced in the tissue and the skin oxygen tension was recorded over approximately 10 s (figure 1(B), time frame IV). Finally, the microelectrode was removed from the tissue (figure 1(B), time frame V). In summary, experiments using the Clark-type electrode revealed that the mean $p_{ti}O_2$ in the footpad of mice is 35.6 ± 13.4 Torr (mean ± standard deviation; $n = 7$; table 1).

Table 1. Skin oxygen level.

Method	(%) O_2	pO_2 (Torr)
Clark	4.8 ± 1.8[a,b]	35.6 ± 13.4[a,b]
LLI	5.5 ± 0.9[a,b]	40.8 ± 6.7[a,b]
RLI	5.4 ± 0.8[a,b]	40.1 ± 5.9[a,b]

[a] Mean ± SD.
[b] No significant statistical difference between groups as tested by ANOVA.

However, oxygen measurements using the polarographic electrode have some serious drawbacks. Although they provide good and reliable mean values of the oxygen tension, they may not be the best tool to measure tissue oxygenation for following main reasons: (a) the electrode will destroy vessels in tissue, and thus harm tissue perfusion; (b) tissue damage upon insertion of the electrode will result in reflex vasodilation of blood vessels in the vicinity of

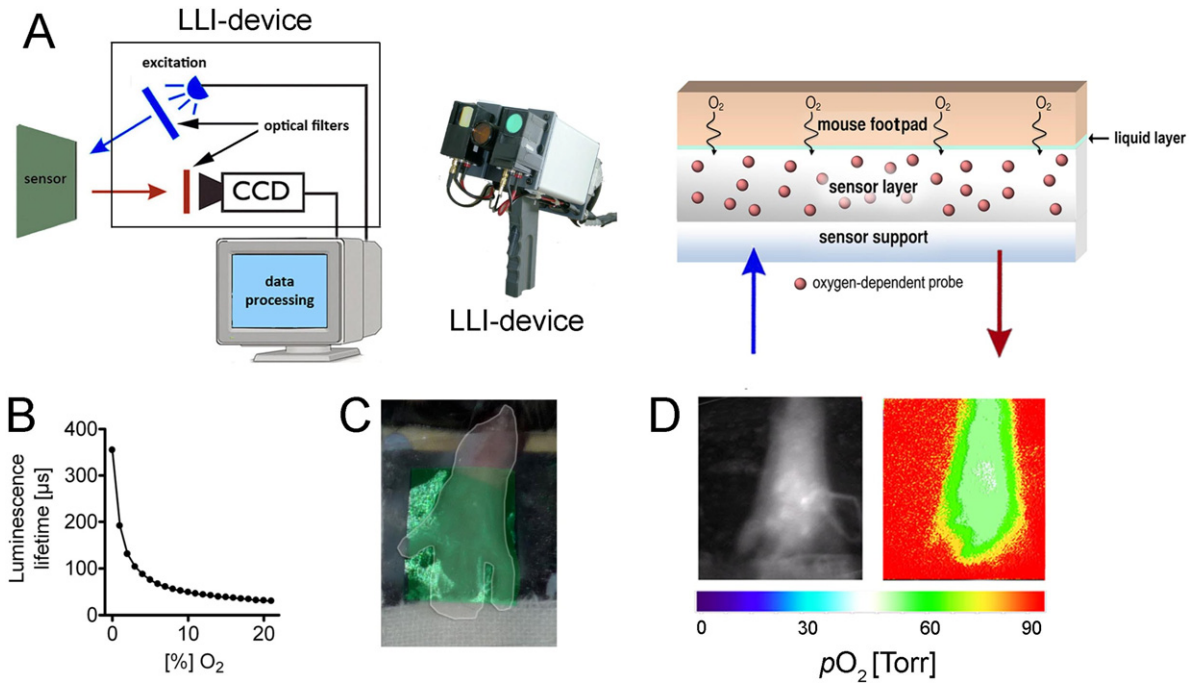

Figure 2. Determination of skin oxygenation using luminescent optical sensor foils with LLI-based imaging technology. (A) Experimental setup to determine skin oxygenation using the LLI-based imaging technology. The measuring setup consists of an optical sensor foil and a portable LLI-instrument. The LLI-device excites the sensor foils with a pulsable LED array (blue light). Subsequent to the pulse of excitation light, the oxygen-dependent decay of the red light emitted from the sensor foil will be recorded by the LLI-device with the use of a time-gated CCD camera. The LLI-device is connected to a PC unit for data acquisition and processing. The transparent sensor foil consists of a sensor layer, which comprises an oxygen-dependent probe immobilized in a highly oxygen-permeable polymer matrix. This sensor layer is immobilized on a transparent and oxygen-blocking polyester support, which guarantees that the sensor detects only oxygen on the side of the sensor layer. To ensure direct contact between the sensor foil and the mouse footpad, a drop of water was added. (B) The LLI-sensor foil used in this study was calibrated at different (%) O_2-values generated by a gas-mixing device. The luminescence decay time τ is given at different (%) O_2-values. Data are mean $\pm$ SD of four measurements. SDs are not discernible since they fall within the limits of the data points. (C) LLI-sensor foil (green) on the footpad (white edging) of a hind leg of a restrained mouse that is positioned on a heating foil (black). (D) A representative black and white intensity image of the sensor (left) and the corresponding referenced pseudocolour image (right) of the calculated skin tissue oxygen distribution.

the electrode [36]; (c) due to tissue injury needle electrode measurements cannot be performed in a repetitive manner; (d) the electrode itself consumes oxygen and thereby alters its oxygen microenvironment during the measurement; (e) the electrode allows only one-spot measurements at a time, thus rastering surfaces to gain 2D-oxygen distributions is very tedious.

3.2. Determination of skin oxygenation using luminescent optical sensor foils along with luminescence-lifetime imaging (LLI)-based imaging technology

Oxygen-sensing with the LLI-device is based on the well-established luminescence quenching technique. This technique uses luminescence lifetime in order to obtain a referenced oxygen-dependent image. The interaction between oxygen and each oxygen-dependent indicator molecule resulted in the quenching of the probes' luminescence, because the energy of the excited dyes is transferred to oxygen molecules by collision. Generally, LLI measures the oxygen-dependent change in the luminescent lifetime, or decay time of luminescent triplet emitters [37] (figures 2(A) and (B)). Luminescent sensor foils for LLI-based imaging were placed on the skin of the footpads of mice (figure 2(C)). Subsequently, LLI imaging was performed (exemplary measurement depicted in figure 2(D)) in order to determine the transcutaneous skin oxygen tension ($p_{tc}O_2$). Due to the anatomy of the vessels in the footpad we could not discern microvessels in the footpads. In summary, these experiments revealed that the mean $p_{tc}O_2$ of the footpad is 40.8 $\pm$ 6.7 Torr (mean $\pm$ standard deviation; $n = 14$; table 1).

3.3. Determination of skin oxygenation using ratiometric luminescence imaging (RLI) technology

Usually, there are three ways to achieve ratiometric oxygen-sensing: combination of luminescence from LED light source and oxygen-sensitive emissive material, mixture of different emissive materials, and dual fluorescent/phosphorescent materials [27]. In this study the sensor foil for RLI consisted of a red luminescent oxygen-dependent probe and a green luminescent reference dye both immobilized in a highly oxygen-permeable polymer matrix to form a sensor layer. Another approach to fabricate the sensor layer would be to use dual fluorescent/phosphorescent polymers [38] or covalently linked sensor layers [39]. Oxygen-sensing with the

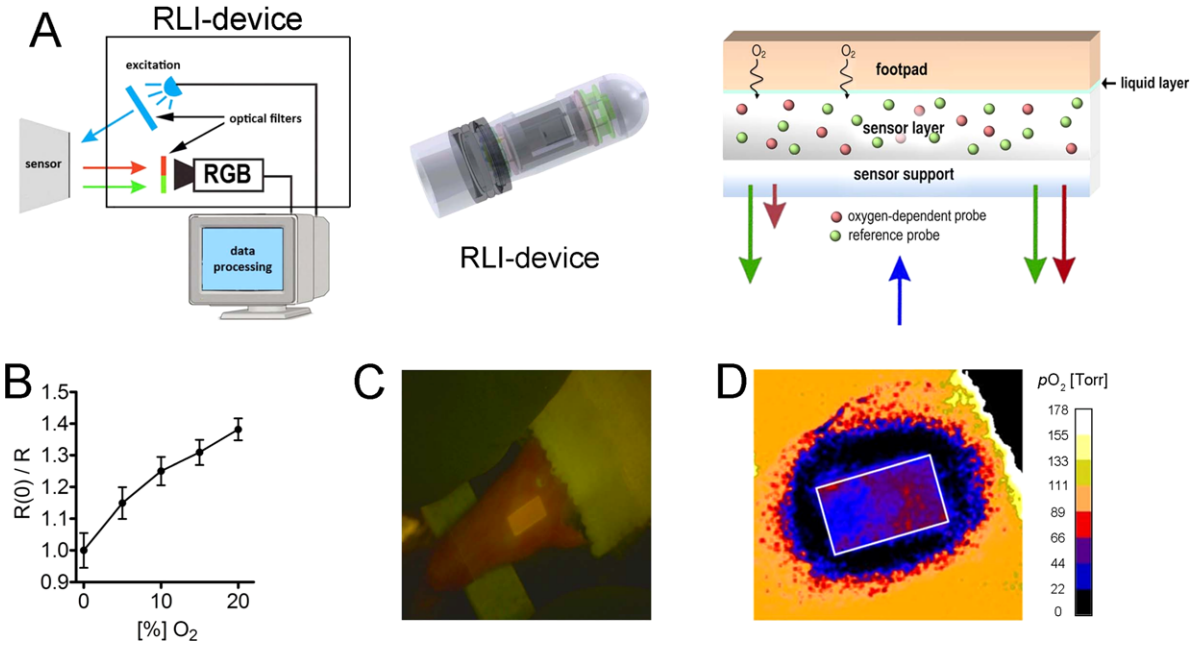

Figure 3. Determination of skin oxygenation using luminescent optical sensor foils with RLI-based imaging technology. (A) Experimental setup to determine skin oxygenation with RLI-based imaging technology. Measurement setup consists of an optical sensor foil, a USB-connected portable RLI-device that is able to excite the sensor foils with LEDs (blue light) and to record the red and green light emitted from the sensor foils with a RGB-chip. The RLI-device is connected to a PC unit for data acquisition and processing. The transparent sensor foil consists of a sensor layer which comprises an oxygen-dependent probe and a reference dye both immobilized in a highly oxygen-permeable polymer matrix. This sensor layer is fixed on an oxygen-blocking polyester support. This guarantees that the sensor detects only oxygen on the side of the sensor layer. To ensure direct contact between the sensor foil and the mouse footpad, a drop of water was added. After excitation with blue light, the reference probe will emit green light and the oxygen-dependent probe will be quenched depending on the oxygen present. (B) The RLI-sensor foil used in this study was calibrated at different (%) O_2-values generated by a gas-mixing device. The emission of the indicator emission in the red channel is divided by the reference emission obtained in the green channel. R(0): ratio red/green at 0% O_2, R: ratio red/green at given (%) O_2. Stern–Volmer calibration plot ($R(0)/R$) of the used RLI-sensor foil is given. (C) RLI-sensor foil on the footpad of a mouse. (D) Representative pseudocolour image of skin tissue oxygen distribution.

RLI-device is based on the measurement of luminescence intensity of the reference dye and the oxygen-dependent probe that is quenched by molecular oxygen. The RLI-device records both wavelengths within one picture at the same time. The signal ratio of these two emitted colors of the sensor foil is calibrated towards its oxygen response [40]. In order to obtain a referenced oxygen-dependent image the camera internally segregates the two signals and calculates the ratio (thus the pO_2) for every recorded pixel (figures 3(A) and (B)). Luminescent sensor foils for RLI were placed on the skin of the mouse footpads (figure 3(C)). Ratiometric luminescence imaging was performed in order to determine $p_{tc}O_2$ of the mouse footpads (figures 3(C) and (D)) using a portable RLI-device. These experiments revealed a mean $p_{tc}O_2$ of 40.1 ± 5.9 Torr (mean $\pm$ standard deviation; $n = 16$; table 1).

When performing statistical analysis there was no significant difference observed between the Clark-type microelectrode measurements and both sensor foil-based oxygen imaging technologies. Nevertheless, we cannot exclude that oxygen-impermeable sensor films and water on skin surface may reduce oxygen supply from air and hence skin tissue oxygenation in a very subtle degree that is not discernible by the oxygen measurement set-ups applied in our study. In contrast to amperometric detection of oxygen, LLI- and RLI can be easily performed. Both are based on sensor foil technology and have the advantage that, due to their transparency the underlying skin structures may also be visualized. These imaging techniques are able to record thousands of measurement positions simultaneously within one measurement, which allows for (a) 2D-mapping of the oxygen tension and possible detection of regions with varying oxygen content; (b) repetitive and non-invasive analysis of tissue oxygenation over time; and thus (c) for constantly monitoring intermittent changes in oxygen tension caused by external stimulus. Both, RLI and LLI as optical readout technologies, are insensitive to inhomogenous or reflective excitation light and drifts in the intensity of light sources and photodetectors. However with RLI, differential photobleaching of the reference and indicator dye, as well as strong colored absorption of the measured tissue might cause problems. Nevertheless, RLI-systems simultaneously detect the signals at the very same time, are by far less sophisticated and expensive than LLI-systems that cost at least $10 000, and are much easier to implement [41].

3.4. Exposure to hypoxia results in a transient drop of tissue oxygenation

Our observation that skin displays mild hypoxia is in excellent accordance with several publications that assessed skin

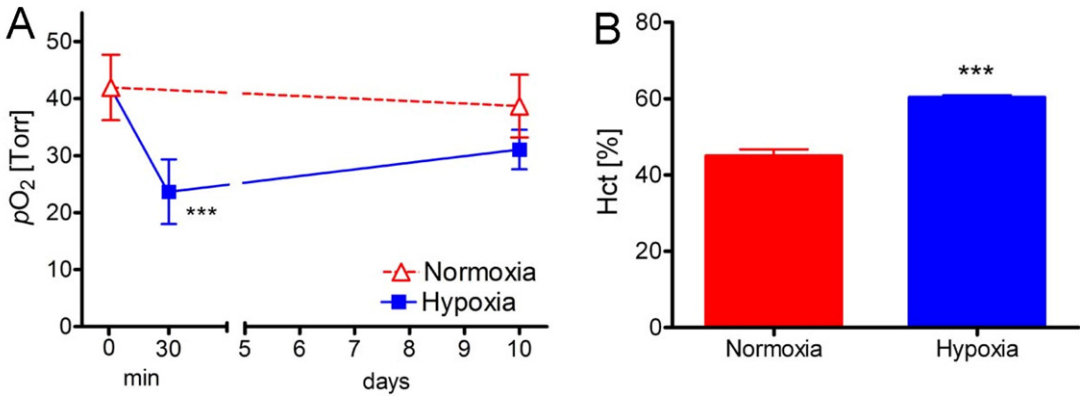

Figure 4. Determination of skin oxygenation using luminescent optical sensor foils with RLI-based imaging technology under conditions of chronic hypoxia. Mice were either subjected to normoxic conditions (normoxia) or normobaric hypoxia by reducing the fractional inhaled O_2 from ambient air (normoxia) to 9% (hypoxia). (A) $p_{tc}O_2$ of hind footpads of mice subjected to normoxic and hypoxic conditions was determined using oxygen-sensor foils and RLI-based imaging technology after 30 min and 10 days. Statistical analysis was performed using the Student's *t* test. *** indicates $P < 0.001$. Data are representative of at least two similar experiments. (B) After 3 days of hypoxic challenge, hematocrit (Hct) values were determined. Statistical analysis was performed using the Student's *t* test. *** indicates $P < 0.001$.

oxygenation using nitroimidazol–adduct formation [42, 43], polarographic electrodes [30, 33, 44], electron paramagnetic resonance [45] and oxygen-sensitive luminescent probes coupled to albumin [46–48] as well as transcutaneous sensor foils using LLI as readout [49]. Earlier studies in humans suggested that systemic hypoxia may evoke a drop in local skin tissue oxygenation [36]. After evaluation of the RLI setup, we were aiming to test whether RLI is able to detect changes in tissue oxygenation after a systemic hypoxic challenge. The animals were subjected to normobaric hypoxia by reducing the fractional inhaled O_2 from ambient air to 9%. We determined the $p_{tc}O_2$ using oxygen-sensor foils and RLI technology after 30 min and 10 days. After 30 min of hypoxic treatment the $p_{tc}O_2$ dropped from 41.4 ± 5.8 Torr to 23.7 ± 5.7 Torr (figure 4(A)). Upon hypoxic treatment the hematocrit (Hct) values increased from 45.0 ± 1.7% to 60.3 ± 0.6% (figure 4(B)) which was paralleled by an increase of $p_{tc}O_2$ to 31.1 ± 3.5 Torr (figure 4(A)).

This is in line with findings in humans reported by Evans and Naylor [36], who observed that in human volunteers the $p_{tc}O_2$ dropped from ∼53 to ∼36 Torr when the partial pressure of oxygen in inhaled gas was reduced to 10%. The normalization of skin tissue oxygen tension obtained after 10 days of chronic hypoxia may be related to enhanced erythropoiesis [50]. This experiment demonstrated that the sensor foil technology enables repetitive and non-invasive analysis of tissue oxygenation over time. This even allowed for constantly monitoring temporally resolved changes in oxygen tension caused by external effects. In future, intradermal injected near-infrared oxygen-sensitive nanomicelles may augment the armamentarium to monitor mouse skin tissue oxygenation [51, 52].

3.5. Conclusions

We have validated the RLI-based system against a Clark-type microelectrode and a LLI-based system for the determination of skin oxygen tension in mice. Our data demonstrate that transcutaneous imaging of skin oxygen tension with the RLI-based system is superior to LLI-based system or invasive measurements with classical Clark-type microelectrodes. Moreover, the RLI-based oxygen-sensing using sensor foils is very straightforward in application, and allows as a non-invasive method transcutaneous analysis of tissue oxygenation in a repetitive and standardized manner over time.

This technology will advance our understanding of local regulation of skin tissue oxygenation and thereby will pave the avenue for a better understanding of tissue oxygenation on the pathogenesis of cancer, infectious and cardiovascular diseases.

Acknowledgments

This study was supported by grants to JJ (JA 1993/1-1 and 2-1) and RJM (SCHA 1009/7-1) from the Deutsche Forschungsgemeinschaft. X-dW was financially supported by the Alexander von Humboldt foundation (Bonn) through a fellowship.

References

[1] Vaupel P, Hockel M and Mayer A 2007 Detection and characterization of tumor hypoxia using pO_2 histography *Antioxid. Redox Signal* **9** 1221–35
[2] Bertout J A, Patel S A and Simon M C 2008 The impact of O_2 availability on human cancer *Nature Rev. Cancer* **8** 967–75
[3] Eltzschig H K and Eckle T 2011 Ischemia and reperfusion—from mechanism to translation *Nature Med.* **17** 1391–401
[4] Sitkovsky M and Lukashev D 2005 Regulation of immune cells by local-tissue oxygen tension: HIF1 alpha and adenosine receptors *Nature Rev. Immunol.* **5** 712–21
[5] Carreau A, El Hafny-Rahbi B, Matejuk A, Grillon C and Kieda C 2011 Why is the partial oxygen pressure of human tissues a crucial parameter? Small molecules and hypoxia *J. Cell. Mol. Med.* **15** 1239–53
[6] Gambhir S S 2002 Molecular imaging of cancer with positron emission tomography *Nature Rev. Cancer* **2** 683–93

[7] Krishna M C, Matsumoto S, Yasui H, Saito K, Devasahayam N, Subramanian S and Mitchell J B 2012 Electron paramagnetic resonance imaging of tumor pO(2) *Radiat. Res.* **177** 376–86

[8] Gross M W, Karbach U, Groebe K, Franko A J and Muellerklieser W 1995 Calibration of misonidazole labeling by simultaneous measurement of oxygen-tension and labeling density in multicellular spheroids *Int. J. Cancer* **61** 567–73

[9] Arteel G E, Thurman R G, Yates J M and Raleigh J A 1995 Evidence that hypoxia markers detect oxygen gradients in liver: pimonidazole and retrograde perfusion of rat liver *Br. J. Cancer* **72** 889–95

[10] Mueller-Klieser W, Schlenger K H, Walenta S, Gross M, Karbach U, Hoeckel M and Vaupel P 1991 Pathophysiological approaches to identifying tumor hypoxia in patients *Radiother. Oncol.* **20** (Suppl. 1) 21–8

[11] Chou S C, Azuma Y, Varia M A and Raleigh J A 2004 Evidence that involucrin, a marker for differentiation, is oxygen regulated in human squamous cell carcinomas *Br. J. Cancer* **90** 728–35

[12] Samoszuk M K, Walter J and Mechetner E 2004 Improved immunohistochemical method for detecting hypoxia gradients in mouse tissues and tumors *J. Histochem. Cytochem.* **52** 837–9

[13] Schreml S, Szeimies R M, Prantl L, Karrer S, Landthaler M and Babilas P 2010 Oxygen in acute and chronic wound healing *Br. J. Dermatol.* **163** 257–68

[14] Tsai A G, Johnson P C and Intaglietta M 2003 Oxygen gradients in the microcirculation *Physiol. Rev.* **83** 933–63

[15] Clark L C Jr, Wolf R, Granger D and Taylor Z 1953 Continuous recording of blood oxygen tensions by polarography *J. Appl. Physiol.* **6** 189–93

[16] Whalen W J, Riley J and Nair P 1967 A microelectrode for measuring intracellular PO_2 *J. Appl. Physiol.* **23** 798–801

[17] Vanderkooi J M, Maniara G, Green T J and Wilson D F 1987 An optical method for measurement of dioxygen concentration based upon quenching of phosphorescence *J. Biol. Chem.* **262** 5476–82

[18] Rumsey W L, Vanderkooi J M and Wilson D F 1988 Imaging of phosphorescence: a novel method for measuring oxygen distribution in perfused tissue *Science* **241** 1649–51

[19] Holst G and Grunwald B 2001 Luminescence lifetime imaging with transparent oxygen optodes *Sensors Actuators* B **74** 78–90

[20] Stich M I, Fischer L H and Wolfbeis O S 2010 Multiple fluorescent chemical sensing and imaging *Chem. Soc. Rev.* **39** 3102–14

[21] Hartmann P, Ziegler W, Holst G and Lubbers D W 1997 Oxygen flux fluorescence lifetime imaging *Sensors Actuators* B **38** 110–5

[22] Stucker M, Schulze L, Pott G, Hartmann P, Lubbers D W, Rochling A and Altmeyer P 1998 FLIM of luminescent oxygen sensors: clinical applications and results *Sensors Actuators* B **51** 171–5

[23] Liebsch G, Klimant I, Frank G, Holst G and Wolfbeis O S 2000 *Appl. Spectrosc.* **54** 548–59

[24] Wang X D, Meier R J, Link M and Wolfbeis O S 2010 Photographing oxygen distribution *Angew. Chem. Int. Edn Engl.* **49** 4907–9

[25] Ungerböck B, Mistlgerger G, Charwat V, Ertl P and Mayr T 2010 Oxygen imaging in microfluidic devices with optical sensors applying color cameras *Procedia Eng.* 456–9

[26] Meier R J, Schreml S, Wang X D, Landthaler M, Babilas P and Wolfbeis O S 2011 Simultaneous photographing of oxygen and pH *in vivo* using sensor films *Angew. Chem. Int. Edn Engl.* **50** 10893–6

[27] Feng Y, Cheng J H, Zhou L, Zhou X G and Xiang H F 2012 Ratiometric optical oxygen sensing: a review in respect of material design *Analyst* **137** 4885–901

[28] Sakadzic S *et al* 2010 Two-photon high-resolution measurement of partial pressure of oxygen in cerebral vasculature and tissue *Nature Methods* **7** 755–9

[29] Wolfbeis O S 2008 Sensor paints *Adv. Mater.* **20** 3759–63

[30] Eickhoff J, Ishihara S and Jacobsen E 1979 P_aO_2 by skin electrode *Lancet* **2** 1188–9

[31] Dowd G S, Linge K and Bentley G 1982 Transcutaneous PO_2 measurement in skin ischaemia *Lancet* **1** 48

[32] Beran A V, Tolle C D and Huxtable R F 1981 Cutaneous blood flow and its relationship to transcutaneous O_2/CO_2 measurements *Crit. Care Med.* **9** 736–41

[33] Sheffield P J 1988 Tissue oxygen measurements *Problem Wounds* ed J C Davis and T K Hunt (New York: Elsevier) pp 17–52

[34] Babilas P, Lamby P, Prantl L, Schreml S, Jung E M, Liebsch G, Wolfbeis O S, Landthaler M, Szeimies R M and Abels C 2008 Transcutaneous pO_2 imaging during tourniquet-induced forearm ischemia using planar optical oxygen sensors *Skin Res. Technol.* **14** 304–11

[35] Schreml S, Meier R J, Wolfbeis O S, Maisch T, Szeimies R M, Landthaler M, Regensburger J, Santarelli F, Klimant I and Babilas P 2011 2D luminescence imaging of physiological wound oxygenation *Exp. Dermatol.* **20** 550–4

[36] Evans N T and Naylor P F 1966 Steady states of oxygen tension in human dermis *Respir. Physiol.* **2** 46–60

[37] Amao Y 2003 Probes and polymers for optical sensing of oxygen *Microchim. Acta* **143** 1–12

[38] Xiang H, Zhou L, Feng Y, Cheng J, Wu D and Zhou X 2012 Tunable fluorescent/phosphorescent platinum(II) porphyrin-fluorene copolymers for ratiometric dual emissive oxygen sensing *Inorg. Chem.* **51** 5208–12

[39] Tian Y Q, Shumway B R and Meldrum D R 2010 A new cross-linkable oxygen sensor covalently bonded into poly(2-hydroxyethyl methacrylate)-co-polyacrylamide thin film for dissolved oxygen sensing *Chem. Mater.* **22** 2069–78

[40] Tschiersch H, Liebsch G, Borisjuk L, Stangelmayer A and Rolletschek H 2012 An imaging method for oxygen distribution, respiration and photosynthesis at a microscopic level of resolution *New Phytol.* **196** 926–36

[41] Meier R J, Fischer L H, Wolfbeis O S and Schaferling M 2013 Referenced luminescent sensing and imaging with digital color cameras: a comparative study *Sensors Actuators* B **177** 500–6

[42] Stewart F A, Denekamp J and Randhawa V S 1982 Skin sensitization by misonidazole: a demonstration of uniform mild hypoxia *Br. J. Cancer* **45** 869–77

[43] Evans S M, Schrlau A E, Chalian A A, Zhang P and Koch C J 2006 Oxygen levels in normal and previously irradiated human skin as assessed by EF5 binding *J. Invest. Dermatol.* **126** 2596–606

[44] Evans N T and Naylor P F 1967 The systemic oxygen supply to the surface of human skin *Respir. Physiol.* **3** 21–37

[45] Krzic M, Sentjurc M and Kristl J 2001 Improved skin oxygenation after benzyl nicotinate application in different carriers as measured by EPR oximetry *in vivo J. Control. Release* **70** 203–11

[46] Buerk D G, Tsai A G, Intaglietta M and Johnson P C 1998 Comparing tissue PO_2 measurements by recessed microelectrode and phosphorescence quenching *Adv. Exp. Med. Biol.* **454** 367–74

[47] Buerk D G, Tsai A G, Intaglietta M and Johnson P C 1998 *In vivo* tissue pO_2 measurements in hamster skinfold by recessed pO_2 microelectrodes and phosphorescence quenching are in agreement *Microcirculation* **5** 219–25

[48] Intaglietta M, Johnson P C and Winslow R M 1996 Microvascular and tissue oxygen distribution *Cardiovasc. Res.* **32** 632–43

[49] Babilas P, Liebsch G, Schacht V, Klimant I, Wolfbeis O S, Szeimies R M and Abels C 2005 *In vivo* phosphorescence imaging of pO_2 using planar oxygen sensors *Microcirculation* **12** 477–87

[50] Haase V H 2013 Regulation of erythropoiesis by hypoxia-inducible factors *Blood Rev.* **27** 41–53

[51] Xiang H, Cheng J, Ma X, Zhou X and Chruma J J 2013 Near-infrared phosphorescence: materials and applications *Chem. Soc. Rev.* **42** 6128–85

[52] Kumar R, Ohulchanskyy T Y, Roy I, Gupta S K, Borek C, Thompson M E and Prasad P N 2009 Near-infrared phosphorescent polymeric nanomicelles: efficient optical probes for tumor imaging and detection *ACS Appl. Mater. Inter.* **1** 1474–81